J Mater Sci (2013) 48:172–177
DOI 10.1007/s10853-012-6725-3

$ZnAl_2O_4$ co-doped with Yb^{3+}/Er^{3+} prepared by combustion reaction: evaluation of photophysical properties

A. C. F. M. Costa · R. H. G. A. Kiminami · P. T. A. Santos · J. F. Silva

Received: 2 April 2012 / Accepted: 5 July 2012 / Published online: 24 July 2012

Abstract Zinc aluminate co-doped with Yb^{3+}/Er^{3+} for potential application in upconversion lasers was prepared in proportions of 2:1, 5:1, and 10:1 by combustion reaction. The samples were characterized by X-ray diffraction, transmission electron microscopy, and optical spectroscopy. The results reveal the formation of crystalline $ZnAl_2O_4$ primary phase and trace amounts of ZnO and $Yb_3Al_5O_{12}$ secondary phases. They also indicate that increasing the Yb^{3+}/Er^{3+} ratio favored the increase of secondary phases. The optical spectroscopy analysis revealed that red emission predominated over green, and that emission intensity was directly influenced by the infrared intensity of the diode laser. These results indicate that $ZnAl_2O_4$ doped with rare earth ions may also be an interesting material for luminescence obtained by energy upconversion.

Introduction

Semiconductor nanocrystals doped with rare earth ions have been investigated extensively in recent years. These materials show interesting enhanced optical properties with potential applications in the design of optoelectronic materials and as efficient phosphor materials for flat-panel displays [1, 2]. This semiconductor matrix co-doped and/or doped with rare earth ions has become increasingly interesting for these technological applications operating in the visible infrared (IR)-excited band. To date, a variety of semiconductor compositions co-doped with Er^{3+} e Yb^{3+} ions have been investigated for the possible application of their optical properties in telecommunications, e.g., in optical amplifiers operating by energy transfer (ET) upconversion [3]. Emission mechanisms have been investigated exhaustively in several hosts in different ceramic matrices [4, 5].

Some of the most relevant works pertaining to this field of investigation are studies on ET and upconversion luminescence in Er/Yb co-doped transparent glass–ceramics containing YF_3 nanocrystals [6]; the upconversion luminescence properties of LaF_3:Yb^{3+}, Er^{3+} nanocrystals, and investigations into the effect of excitation power density on the upconversion luminescence of LaF_3:Yb^{3+}, Er^{3+} nanocrystals [7]; the Judd–Ofelt analyses and luminescence of Er^{3+}/Yb^{3+} co-doped transparent glass–ceramics containing $NaYF_4$ nanocrystals reported by Ping et al. [8]; the preparation and spectroscopic properties of nanostructured glass–ceramics containing Yb^{3+}, Er^{3+} ions and Co^{2+}-doped $MgAl_2O_4$ nanocrystals described by Chen et al. [9]; and You et al.'s [10] study of the upconversion properties of Yb^{3+} and Er^{3+} doped $Y_4Al_2O_9$ phosphors.

Among these various types of matrices, aluminum-based spinels are an interesting type of oxide ceramics with significant technological applications, a fact that has motivated several research groups to focus their efforts on the synthesis and characterization of rare earth-doped $ZnAl_2O_4$ phosphors. Some of the most relevant papers on this subject include ultrafine gahnite ($ZnAl_2O_4$) nanocrystals: hydrothermal synthesis and photoluminescent properties reported by Chen et al. [11]; the work of Menon et al. [12], who evaluated the thermally stimulated luminescence and optically stimulated luminescence properties of Tb-doped

A. C. F. M. Costa · P. T. A. Santos · J. F. Silva
Department of Materials Engineering, Federal University of Campina Grande, Campina Grande, PB 58429-900, Brazil

R. H. G. A. Kiminami (✉)
Department of Materials Engineering, Federal University of São Carlos, São Carlos, SP 13565-190, Brazil
e-mail: ruth@power.ufscar.br

$ZnAl_2O_4$ prepared by combustion synthesis; the preparation of spherical porous $ZnAl_2O_4:Eu^{3+}$ phosphors: PEG-assisted hydrothermal growth and photoluminescence reported by Chen and Ma [13]; and a study of the optical properties of $ZnAl_2O_4:Eu^{3+}$ hollow nanophosphors by Barros et al. [14].

Gahnite ($ZnAl_2O_4$) is a useful semiconductor (3.8 eV) which, in its polycrystalline form, is transparent to visible light at wavelengths of >320 nm. This makes it suitable for use as a transparent conductor and as a dielectric, optical [15], and catalytic material [16]. $ZnAl_2O_4$ has attracted much interest for applications in various fields, including reflective optical coatings in aerospace applications, as a phosphor material, and as an ultraviolet-transport electro-conductive oxide [17].

Rare earth dopants, which normally exist in the form of trivalent ions, show very narrow line fluorescence bands and exhibit a characteristic intra 4f shell luminescence, which is nearly independent of both host material and temperature [18]. $ZnAl_2O_4$ phosphors activated by rare earth metal ions have been studied due to the unique luminescent properties resulting from their high thermal and chemical stability and high emission quantum yields [13] showing a promising potential for use as a host lattice for rare earth ions.

In this context, this study investigated the upconversion luminescence of $ZnAl_2O_4$ co-doped with Yb^{+3}/Er^{3+} ions in proportions of 2:1, 5:1, and 10:1 mol, prepared by combustion reaction, for potential application in lasers.

Experimental

The precursor materials used in this work were zinc nitrate $Zn(NO_3)_2{\cdot}6H_2O$ (Merck), aluminum nitrate $Al(NO_3)_3{\cdot}9H_2O$ (Aldrich), and Er_2O_3 and Yb_2O_3 rare earth oxides (Aldrich), which were used as oxidizers and a source of metallic cations. Urea [$CO(NH_2)_2$] was used as a reducing agent. All the reagents used here were of analytical grade with 98–99.9 % purity. The initial composition of the solution containing the nitrates, oxides, and urea was based on the total valence of the oxidizing reagents and reducing agent, based on the concept of propellant chemistry [19, 20], which considers carbon (+4), hydrogen (+1), aluminum (+3), zinc (+2), ytterbium, and erbium (+3) as reducing elements. Oxygen was considered an oxidizing element with a valence of (−2) and the valence of nitrogen was considered zero because it is inert. The Yb^{3+}/Er^{3+} reagents used for doping the $ZnAl_2O_4$ matrix in ratios of 2:1, 5:1, and 10:1 were weighed and placed in a Pyrex beaker to which 5 mL of distilled water was added to form stoichiometric solutions. These solutions were then heated on a hot plate at 480 °C until they self-ignited. The products of the combustion reaction were then placed in a muffle furnace preheated to 500 °C where they were left for about 15 min to eliminate any remaining volatile compounds (from urea and nitrate decomposition) that might still be present due to the short time of reaction. The resulting porous flake-shaped powders were disagglomerated in a mortar agate, sifted through a 325 mesh (44 μm) sieve, and then characterized. The reaction temperature was measured with a RAYTEK RAYCI IR pyrometer, while the flame combustion temperature was measured with a RAYTEK MA2SC IR pyrometer, and the flame time with a CONDOR digital chronometer. The reactions' explosiveness and flame color were evaluated visually during the experiment.

The samples were characterized by X-ray diffraction (XRD, SHIMADZU 6000, equipped with a Ni filter, using Cu Kα radiation, a scan rate of 2° 2θ/min, in a 2θ range of 10–75°, voltage of 40 mA, in steps of 0.02°, with a step time of 1 s, at room temperature—25 °C). By means of Scherrer's equation [21], the crystallite size was calculated from the broadest peaks of the most intense XRD lines of $ZnAl_2O_4$, which were d(311) d(220) d(440) d(511). The morphology of the samples was then examined by transmission electron microscopy (TEM) (Phillips EM420), operating at 120 kV). The entire spectroscopic characterization of the samples was performed at room temperature. Ground-state absorption (GSA) spectra were measured using a Lambda 900 spectrophotometer (Perkin Elmer) operating in the range of 700–1,700 nm. For these measurements, the samples were ground into powder and pressed into KBr pellets. The upconversion spectra were recorded at 980 nm using a homemade diode laser as the excitation source. The powder samples were placed in capillary tubes and their luminescent signals were filtered using a single monochromator (0.3 m) (Thermo Jarrell Ash 82497). The filtered signals were collected with a photomultiplier (RCA 31034) and amplified with a lock-in amplifier (PAR 128).

Results

Table 1 lists the combustion flame time, combustion flame temperature, and flame color of the reactions. As can be seen, all the samples presented a yellow flame color. The average plate temperature was 531 °C, which is slightly

Table 1 Characteristics of the $ZnAl_2O_4:Yb^{3+}/Er^{3+}$ samples prepared by combustion reaction

Yb^{3+}/Er^{3+} ratio	2:1	5:1	10:1
Combustion flame time (s)	14	18	16
Combustion flame temperature (°C)	727	713	794
Flame color	Yellow	Yellow	Yellow

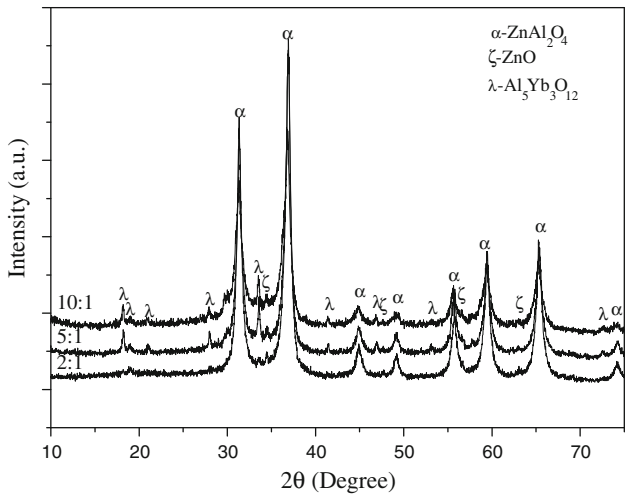

Fig. 1 XRD patterns of $ZnAl_2O_4$ samples co-doped with Yb^{3+}/Er^{3+} prepared by combustion reaction

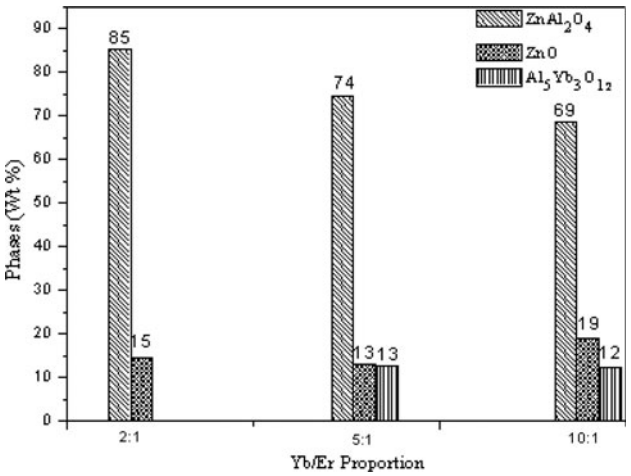

Fig. 2 Phase quantification of the samples containing Yb^{3+}/Er^{3+} ratios of 2:1, 5:1, and 10:1

higher than the maximum temperature of 480 °C recommended by the manufacturer. The slight increase in combustion flame time and temperature was due to the increase in the Yb^{3+}/Er^{3+} ratio.

Figure 1 shows the XRD patterns of the $ZnAl_2O_4$:Yb^{3+}/Er^{3+} samples prepared by combustion reaction and containing Yb^{3+}/Er^{3+} ratios of 2:1, 5:1, and 10:1. These patterns indicate the formation of primary crystalline product $ZnAl_2O_4$ spinel (JCPDS #82-1136) and traces of secondary product ZnO (gahnite) (JCPDS #75-0576) in all the samples. The 10:1 sample also showed the presence of $Yb_3Al_5O_{12}$ (JCPDS #23-1476) product. The calculated crystallite sizes of the primary phase were 14, 16, and 11 nm in the 2:1, 5:1, and 10:1 compositions, respectively. The results indicate a slight decrease in crystallite size with increasing amounts of Yb^{3+}/Er^{3+}. This may have been due to the presence of secondary product, which induced a more marked broadening of the peak and reduction in diffraction peak intensity.

The ionic radius of Yb^{3+} (0.75 Å) and Er^{3+} (0.85 Å) ions differed from the ionic radius of Al^{3+} (0.88 Å) ions by 15 and 3 %, respectively. This indicates that Al^{3+} ions are more easily replaced by Er^{3+} ions than by Yb^{3+} ions. Because the amount of Yb^{3+} used for co-doping was consistently higher than Er^{3+}, and because its radius is 15 % lower than the ionic radius of Al^{3+}, it is expected that increasing the amount of Yb^{3+} in co-doping (Yb^{3+}/Er^{3+}) favors a low solubility limit in the $ZnAl_2O_4$ lattice leading to the formation of secondary product rich in Yb^{3+} ($Al_3Yb_3O_{12}$) as indicated in the XRD pattern.

The presence of primary product $ZnAl_2O_4$ and secondary product ZnO was also reported by Barros et al. [14] in their evaluation of the photophysical properties of Eu^{3+} and Tb^{3+}-doped $ZnAl_2O_4$ phosphors obtained by combustion reaction. The authors stated that even with the presence of second phase, samples containing Eu^{3+} and Tb^{3+} ions displayed red and green photoluminescence, respectively.

Figure 2 quantifies the amount of products determined from the XRD data for the 2:1, 5:1, and 10:1 samples. As can be observed, the 2:1 sample showed the highest percentage of primary product $ZnAl_2O_4$ co-doped with Yb^{3+}/Er^{3+} (85 %) and 15 % of secondary product ZnO. The 5:1 and 10:1 compositions showed a high percentage of primary product $ZnAl_2O_4$ co-doped with Yb^{3+}/Er^{3+} and the presence of two secondary products. However, increasing the ratio of Yb^{3+} relative to Er^{3+} increased the percentage of secondary product ZnO, thereby reducing the concentration of the spinel phase.

Figure 3 shows bright field TEM micrographs of $ZnAl_2O_4$ co-doped with Yb^{3+}/Er^{3+} in ratios of 2:1 and 5:1. Figure 3a (sample 2:1) reveals a highly homogeneous morphology of approximately hexagonal particles. In contrast, the morphology of sample 5:1 (Fig. 3b) is heterogeneous consisting of particles of different sizes and shapes, most of them approximately hexagonal. The average particle sizes of samples 2:1 and 5:1 are 7 and 28 nm, respectively. The particle size determined by TEM confirms the efficiency of the combustion synthesis reaction in producing nanoparticles, which tend to agglomerate due to their high reactivity (high surface energy).

Figure 4 shows the spectra of $ZnAl_2O_4$ co-doped with Yb^{3+}/Er^{3+} in ratios of 2:1, 5:1, and 10:1 recorded using IR excitation wavelengths below 980 nm at room temperature. As can be observed, at wavelengths below 980 nm and near IR excitation, these samples show three well-defined, but low intensity, emission peaks at 525, 550, and 655 nm. The green emissions at 525 and 550 nm were attributed to $^2H_{11/2} \rightarrow {}^4I_{15/2}$ and $^2S_{3/2} \rightarrow {}^4I_{15/2}$ transitions, respectively, while the red emission at 655 nm was attributed to the

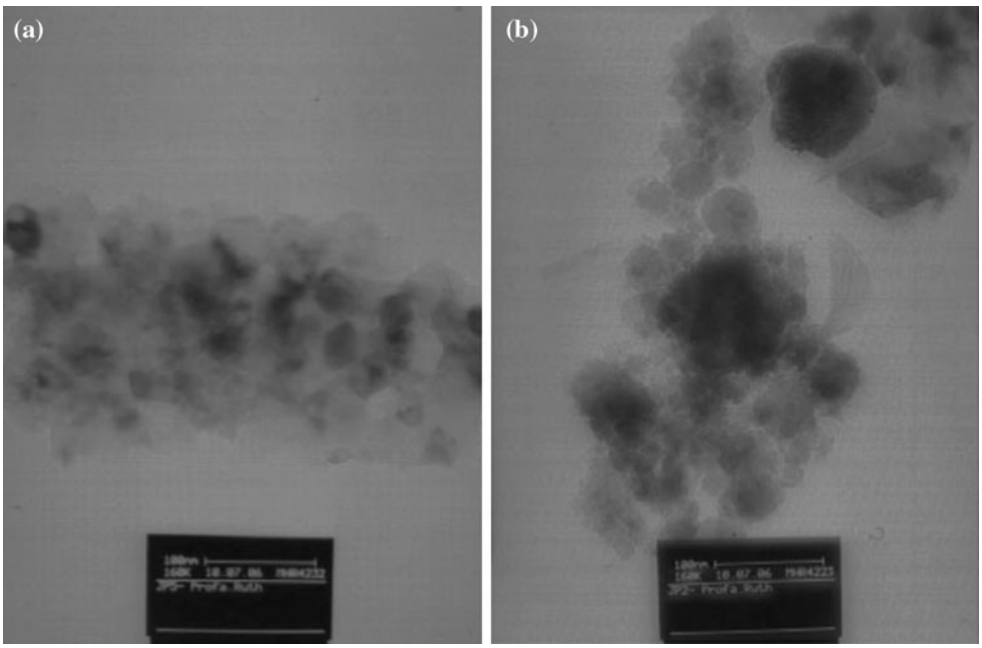

Fig. 3 TEM *micrographs* of the $ZnAl_2O_4$ samples co-doped with Yb^{3+}/Er^{3+} prepared by combustion reaction: **a** 2:1 ratio and **b** 5:1 ratio

$^4F_{9/2} \rightarrow {}^4I_{15/2}$ transition. The same behavior was reported by Qu et al. [7] in their study of the effect of excitation power density on the upconversion luminescence of $LaF_3:Yb^{3+}$, Er^{3+} nanocrystals. The 5:1 composition shows much more intense $^4F_{9/2} \rightarrow {}^4I_{15/2}$ ($\sim$655 nm) type transitions to red than the 2:1 composition, and very weak emission attributed to $^2H_{11/2} \rightarrow {}^4I_{15/2}$ ($\sim$525 nm), $^2S_{3/2} \rightarrow {}^4I_{15/2}$ ($\sim$550 nm) transitions to green. It was found that increasing the proportion of Yb^{3+} from 5:1 to 10:1 while maintaining a constant proportion of Er^{3+} (sample 10:1) gave rise to the transition $^4F_{9/2} \rightarrow {}^4I_{15/2}$, but with a lower intensity than in sample 5:1.

As Fig. 4 indicates, the emission spectrum of the 5:1 composition reveals transition characteristic of Er^{3+} ions centered at 655 nm ($^4F_{9/2} \leftrightarrow {}^4I_{15/2}$) and Yb^{3+} ions centered at 550 nm ($^2F_{5/2} \leftrightarrow {}^2F_{7/2}$). The 10:1 composition shows a decline in the intensity of luminescence resulting from the decrease in the distance between the dopant (activator) and the array, causing the migration of excitation energy among resonant ions of the same species, in this case Er^{3+} ions. This cross-relaxation (CR) mechanism causes a large amount of energy to dissipate in the form of non-radiative energy. It seems unlikely that CR had any effect at low concentrations in view of the large distance between actuators hindering the transfer of energy between them.

Figure 5 shows the room temperature upconversion spectra of the 5:1 composition in response to increasing excitation IR diode laser power. The spectrum of the conversion occurring in the region of 500–580 nm of the sample was visible at about 500–575 nm. It was found that when the excitation power density increased to a higher

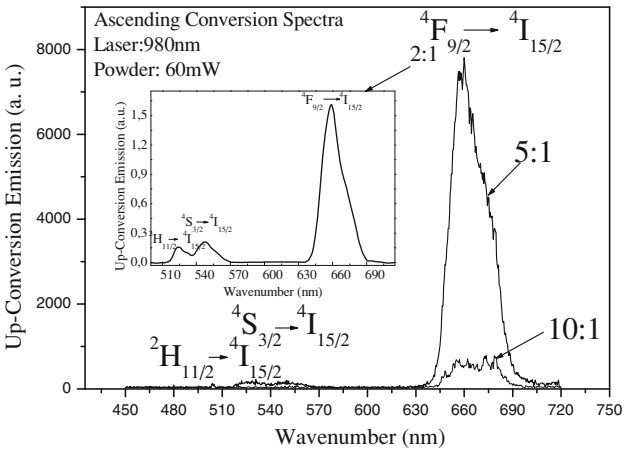

Fig. 4 Upconversion emission spectra of $ZnAl_2O_4$ samples co-doped with Yb^{3+}/Er^{3+}

region, the intensities of green and red emission increased rapidly in response to increasing excitation power. Increasing the laser power augmented the temperature of the system causing the maximum emission bands at around 655 nm to increase and hence, increasingly favoring the $^4F_{9/2} \rightarrow {}^4I_{15/2}$ transitions.

In the frequency upconversion process, the upconversion emission intensity I_{up} increases in proportion to the nth power of IR excitation intensity, I_{IR}, i.e.,

$$I_{up} \propto I_{IR}^{n}$$

where n is the number of IR photons absorbed per visible photon emitted. A plot of log I_{up} versus log I_{IR} yields a straight line with slope n. Figure 6 shows such a plot for

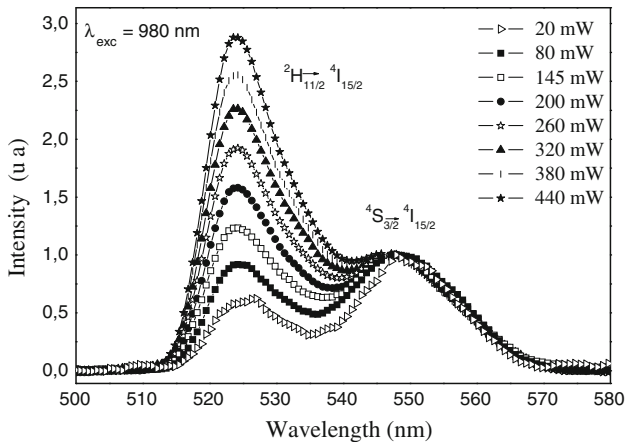

Fig. 5 Upconversion fluorescence spectra of $ZnAl_2O_4$ co-doped with a 5:1 ratio of Yb^{3+}/Er^{3+} recorded at 980 nm of excitation laser power

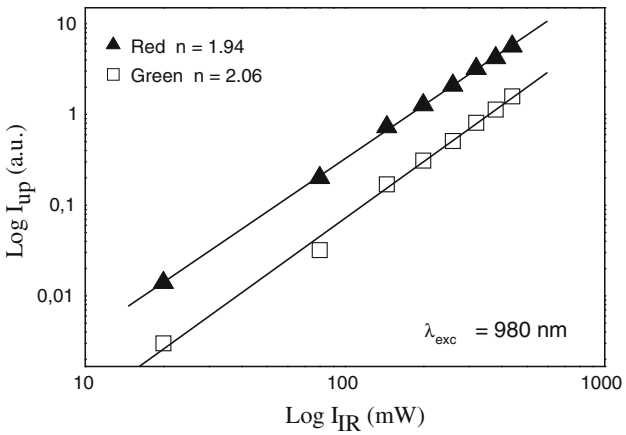

Fig. 6 Dependence of upconversion fluorescence intensity on 980 nm excitation power in $ZnAl_2O_4$ samples co-doped with Yb^{3+}/Er^{3+}

the zinc aluminate co-doped with a 5:1 ratio of Yb^{3+}/Er^{3+} under 980 nm excitation. At both emission intensities in the region of green and red wavelengths, note the linear dependence on increasing laser power showing slope coefficients of 2.6 and 1.94 obtained for green and red emissions, respectively. These results indicate that a two-photon process populates the $^4S_{3/2}$, the $^2H_{11/2}$, and the $^4F_{9/2}$ levels. Similar results were reported by Sun et al. [22], who evaluated the optical transitions and frequency upconversion fluorescence of Er^{3+}/Yb^{3+} co-doped strontium–lead–bismuth glasses. The authors observed intense green and red emissions centered at 525, 546, and 657 nm in response to 975 nm excitation, which corresponded, respectively, to transitions $^2H_{11/2} \rightarrow {}^4I_{15/2}$, $^2S_{3/2} \rightarrow {}^4I_{15/2}$, and $^4F_{9/2} \rightarrow {}^4I_{15/2}$, and reported that they obtained values of 1.87, 1.89, and 1.86 for *n* corresponding to the 525, 546, and 657 nm emission bands, respectively.

An analysis of the effect of co-doping with a 5:1 ratio of Yb^{3+}/Er^{3+} ions indicated that the transition of $^2H_{11/2} \rightarrow {}^4I_{15/2}$ to green from the Yb^{3+} ions led to much lower upconversion intensity than that obtained with Er^{3+} ions in the transition of $^4F_{9/2} \rightarrow {}^4I_{15/2}$ to red. Therefore, the emission intensity of green luminescence does not exceed the red emission in the samples with a 5:1 ratio of Yb^{3+}/Er^{3+}.

As Fig. 6 indicates, the upconversion intensity of red emission showed a rapid growth on the upward line exceeding the green emission when co-doping with a 5:1 ratio of Yb^{3+}/Er^{3+}. This predominance of red emission over green emission was also observed by Wang et al. [23] in their study of the upconversion energy of Er^{3+} ions in ZnO nanocrystals produced by two-photon energy.

According to energy matching and the quadratic dependence on excitation power, the possible upconversion mechanisms for the emissions are discussed based on the simplified energy levels of Er^{3+} and Yb^{3+} presented in Fig. 7. For the green emissions, in the first step, the $^4I_{11/2}$ level is directly excited with 980 nm light by GSA and/or by ET from the $^2F_{5/2}$ level of Yb^{3+}:$^2F_{5/2}(Yb^{3+}) + {}^4I_{15/2}(Er^{3+}) \rightarrow {}^2F_{7/2}(Yb^{3+}) + {}^4I_{11/2}(Er^{3+})$. Since the absorption cross section of Yb^{3+} is much larger than that of Er^{3+} in the 980 nm region, the ET mechanism predominates at the excitation level of $^4I_{11/2}$. The second step involves excitation mechanisms based on the long-lived $^4I_{11/2}$ level as follows: CR, $^4I_{11/2}(Er^{3+}) + {}^4I_{11/2}(Er^{3+}) \rightarrow {}^4F_{7/2}(Er^{3+}) + {}^4I_{15/2}(Er^{3+})$; excited-state absorption (ESA), $^4I_{11/2}(Er^{3+})$ + a photon $\rightarrow {}^4F_{7/2}(Er^{3+})$; and ET, $^2F_{5/2}(Yb^{3+}) + {}^4I_{11/2}(Er^{3+}) \rightarrow {}^2F_{7/2}(Yb^{3+}) + {}^4F_{7/2}(Er^{3+})$. The populated Er^{3+} $^4F_{7/2}$ level then relaxes rapidly and continues as follows: ET from Yb^{3+}, $^2F_{5/2}(Yb^{3+}) + {}^4I_{13/2}(Er^{3+}) \rightarrow {}^2F_{7/2}(Yb^{3+}) + {}^4F_{9/2}(Er^{3+})$; CR among Er^{3+} ions, $^4I_{13/2} + {}^4I_{11/2} \rightarrow {}^4I_{15/2} + {}^4F_{9/2}$; ESA, $^4I_{13/2}$+ non-radiatively to the next lower levels $^2H_{11/2}$; and $^4S_{3/2}$ resulting from the small energy gap between them. Er^{3+} ions in the $^2H_{11/2}$ state can also decay into the $^4S_{3/2}$ state due to multiphonon relaxation.

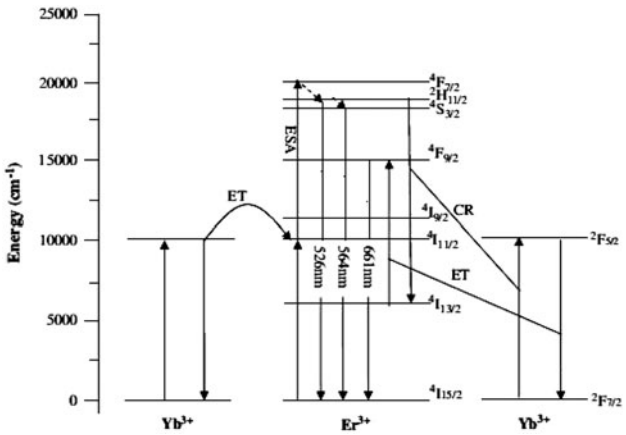

Fig. 7 Simplified *diagram* of the energy level of Er^{3+} and Yb^{3+} ions and possible transition pathways in zinc aluminate co-doped with Er^{3+}/Yb^{3+} [10]

The estimated energy gap between the $^2H_{11/2}$ state and the next lower state $^4S_{3/2}$ is $\sim$800 cm^{-1} [10]. Thus, the multiphoton relaxation rate is very high and the 525 nm emission intensity is reduced. These mechanisms then produce the two $^2H_{11/2} \rightarrow {}^4I_{15/2}$ and $^4S_{3/2} \rightarrow {}^4I_{15/2}$ green emissions centered at 525 and 546 nm, respectively. The red emission at 657 nm originates from the $^4F_{9/2} \rightarrow {}^4I_{15/2}$ transition and the population of $^4F_{9/2}$ is based on the photon $\rightarrow {}^4F_{9/2}$. The $^4I_{13/2}$ level is populated owing to non-radiative relaxation from the upper $^4I_{11/2}$ level. In addition, the non-radiative process from $^4S_{3/2}$ state, which is populated by means of the previously described process to the $^4F_{9/2}$ level, also contributes to the red emission.

Conclusions

Synthesis by combustion reaction was favorable for obtaining $ZnAl_2O_4$ spinel: Yb^{3+}/Er^{3+} with an average crystallite size of 11–16 nm and particle sizes ranging from 7 to 28 nm. IR-to-visible upconversion in zinc aluminate co-doped with Yb^{3+}/Er^{3+} was achieved under continuous excitation at 980 nm at room temperature. The emission spectra of the samples indicated that red luminescence predominated over green in response to IR laser excitation. A comparison of the spectra of upconversion luminescence of all the co-doped compositions indicated that the 10:1 composition showed the lowest relative emission intensity due to self-removal of the ions involved, causing the distance between ions to decrease, which favored the occurrence of CR. The 5:1 composition showed better upconversion emission than the 2:1 and 10:1 compositions, probably due to the good accommodation of Yb^{3+}/Er^{3+} ions in the zinc aluminate, favoring ET between the transition states. Zinc aluminate co-doped with a 5:1 concentration of Yb^{3+}/Er^{3+} with intense upconversion fluorescence can be used as potential host material for upconversion lasers.

Acknowledgements The authors gratefully acknowledge the Brazilian Research Funding Agencies CNPq, RENAMI, FAPESP, and Inct-INAMI for their financial support of this work. We are also indebted to Prof. Luiz Antonio de Oliveira Nunes from the Department of Physics of the University of São Paulo-USP for performing the upconversion tests.

References

1. Feldmann C, Justel T, Ronda CR, Schmidt PJ (2003) Adv Funct Mater 13:511
2. Saines PJ, Elcombe MM, Kennedy BJ (2006) J Solid State Chem 179:613
3. Shanfeng L, Min Z, Yang P, Qingyu Z, Mingshan Z (2010) J Rare Earths 28(2):237
4. Zhou J, Zhang W, Huang T, Wang L, Li J, Liu W, Jiang B, Pan Y, Guo J (2011) Ceram Int 37:513
5. Yang Z, Zhu K, Song Z, Zhou D, Yin Z, Qiu J (2011) J Solid State Commun 151:364
6. Weng F, Chen D, Wang Y, Yu Y, Huang P, Lin H (2009) Ceram Int 35:2619
7. Qu Y, Kong X, Sun Y, Zeng Q, Zhang H (2009) J Alloy Compd 485:493
8. Ping H, Chen D, Yu Y, Wang Y (2010) J Alloy Compd 490:74
9. Chen L, Yu C, Hu L, Chen W (2012) Solid State Sci 14:e287
10. You W, Lai F, Jiang H, Liao J (2012) Physica B 407:1094
11. Chen XY, Ma C, Zhang ZJ, Wang BN (2008) Mater Sci Eng B 151:224
12. Menon S, Dhabekar B, Alagu Rajaa E, More SP, Gundu Raob TK, Kher RK (2008) J Lumin 128:1673
13. Chen XY, Ma C (2010) Opt Mater 32:415
14. Barros BS, Melo PS, Kiminami RHGA, Costa ACFM, Sá GF, Alves S Jr (2006) J Mater Sci 41:4744. doi:10.1007/s10853-006-0035-6
15. Shen SC, Hidajat K, Yu LE, Kawi S (2004) Adv Mater 16:541
16. Farhadi S, Panahandehjoo S (2010) Appl Catal A 382:293
17. Zawadzki M, Wrzyszcz J, Strek W, Hreniak D (2001) J Alloy Compd 323–324:279
18. Singh V, Chakradhar RPS, Rao JL, Kim D-K (2008) J Lumin 128(3):394
19. Jain SR, Adiga KC, Pai Verneker V (1981) Combust Flame 40:71
20. Costa ACFM, Kiminam RHGA, Morelli MR (2009) Handbook of nanoceramics and their based nanodevices, vol 5. American Science Publishers, Valencia, p 80
21. Klung H, Alexander L (1962) X-ray diffraction procedures. Wiley, New York
22. Sun H, Dai S, Xu S, Wen L, Hu L, Jiang ZJ (2004) Mater Lett 58: 3948
23. Wang X, Kong X, Shan G, Yu Y, Sun Y, Feng L, Chao K, Lu S, Li Y (2004) J Phys Chem B 108(48):18408